Check for updates

ADVANCED ENGINEERING MATERIALS
www.aem-journal.com

Anisotropic Wettability Induced by Femtosecond Laser Ablation

*Mostafa Shojaeian, Ali K. Yetisen, and Savas Tasoglu**

Laser ablation has been utilized for locally and selectively modifying the surface wettability of materials in situ and enabling on-demand microfabrication. The anisotropic wettability has been observed on chemical and/or topographical patterns, such as an array of laser-inscribed strips with spacings, created on surfaces during the fabrication process. Herein, the effectiveness of the femtosecond laser ablation is evaluated in selectively modifying surface wettability. The areas processed by laser ablation exhibit anisotropic wetting behavior, even after the laser strips are overlapped. The laser-induced anisotropic surface wettability is present in space governed by laser scanning speed, scan/strip overlap, laser fluence, scan repetition, and bidirectional scanning angle. Moreover, the femtosecond laser ablation process is optimized to enhance the conventional laser inscription, leading to a modified and consistent methodology to achieve cost-effective fabrication.

1. Introduction

Polymers have been widely utilized for the fabrication of microfluidic devices, owing to their low cost, ease of handling, and ability to be modified to exhibit desirable physical, chemical, and optical properties. The surface characteristics of polymers are important in microfluidics, where precise handling of biochemical reagents is crucial. Surface wettability is a key surface characteristic that is determined by the interaction between a liquid and a solid surface. Alteration and/or modification of surface wettability can be achieved through changes in surface chemistry and/or topography. The wetting properties of surfaces play a vital role in both nature and industrial settings. For example, some plants and animals exhibit favorable wetting behaviors that enable them to adapt to their environments and perform their biological functions (e.g., anisotropic wettability).[1] The wetting properties that are independent of the measurement direction are referred to as isotropic wettability. Conversely, the dependency of the wetting properties on the direction is identified as anisotropic wettability at which liquids nonhomogeneously spread over surfaces. The anisotropic wettability could potentially find applications in nano- and microfluidics, biomedical/bioinspired devices, and self-cleaning products.[2]

Anisotropic surfaces can be synthesized through the formation of patterns, which share a common attribute of discontinuity in the chemical or structural (topographical) surface composition. Chemical or physical mechanisms have been also explored to generate surface gradients. For the chemically patterning strategy, photolithography,[3,4] inkjet printing,[5] and selective deposition[6] methods have been utilized. Corresponding surfaces are decorated with patches and/or patterns with distinct chemical properties (e.g., hydrophobicity, hydrophilicity) to achieve chemical heterogeneity on the solid surfaces. The surface chemical dissociation together with the geometry/shape of patterns are dominant parameters. The presence of surface heterogeneities, i.e., patterned features, plays a significant role in the creation of anisotropic wetting characteristics. Nevertheless, some chemical surface modifications may induce minor topographical alterations such as increased surface roughness resulting from oxygen plasma treatment,[7,8] which may influence the modification of surface wettability. In contrast, for the structural patterns, surfaces are artificially modulated by fabricating features of nano- and micrometers (e.g., grooves, strips, pillars). Molding and embossing,[9] imprinting,[10] laser micromachining,[11,12] and metal deposition[13] can be employed to fabricate the structural patterns. The production of directional patterns is a common method for generating anisotropic wetting

M. Shojaeian, S. Tasoglu
Department of Mechanical Engineering
Koç University
Sariyer/Istanbul 34450, Turkiye
E-mail: stasoglu@ku.edu.tr

A. K. Yetisen
Department of Chemical Engineering
Imperial College London
London SW7 2AZ, UK

S. Tasoglu
Koç University Arçelik Research Center for Creative Industries (KUAR)
Koç University
Sariyer/Istanbul 34450, Turkiye

S. Tasoglu
Koç University Research Center for Translational Medicine
Koc University
Sariyer/Istanbul 34450, Turkiye

S. Tasoglu
Boğaziçi Institute of Biomedical Engineering
Boğaziçi University
Çengelköy/Istanbul 34684, Turkiye

The ORCID identification number(s) for the author(s) of this article can be found under https://doi.org/10.1002/adem.202301217.

© 2023 The Authors. Advanced Engineering Materials published by Wiley-VCH GmbH. This is an open access article under the terms of the Creative Commons Attribution License, which permits use, distribution and reproduction in any medium, provided the original work is properly cited.

DOI: 10.1002/adem.202301217

surfaces. Although these patterns exhibit symmetry in both the *x*- and *y*-directions, asymmetry in the surface structures in the *z*-direction or multiple directions can lead to a distinct anisotropic wetting mode, which is characterized by unidirectional wetting. For example, such structures include bent nanopillars[13] and tilted nanorods[14] on the surfaces. The fabrication of anisotropic features on surfaces is a significant aspect of achieving surface wettability. While the desired topographical patterns are often intentionally produced, the anisotropic surfaces can also be an unintended outcome of a fabrication process. In manufacturing processes that involve the manipulation of surface topography, the alteration of surface chemistry may not be a primary concern. Therefore, the surface chemistry may or may not be affected by the structural surface patterning.[15–17]

The study of wettability characteristics of materials has become an increasingly important research area, as advances in fabrication methods have expanded the scope of polymeric materials. In this context, poly(methyl methacrylate) (PMMA) has emerged as a popular material for both industrial and research applications, especially for the fabrication of microfluidic devices. This can be attributed to its advantageous properties, including 1) amenability for injection molding and patterning, and 2) favorable optical properties. Lab-on-a-chip PMMA devices can be fabricated through injection molding and hot embossing. Although these techniques are designed for mass production, their applications in rapid prototyping are not practical. Furthermore, the method of fabrication itself could potentially change the wetting behavior of a surface. A potential fabrication method for creating microstructures (e.g., microchannels) is to exploit laser-based direct writing on various substrates.[18,19] For this purpose, CO_2, excimer, and femtosecond (fs) laser ablation could modify the surface wettability of substrates in addition to facilitating rapid prototyping of microfluidic devices. The absorption of laser irradiation in polymers allows material removal from the inscribed zone at sufficiently large laser energy, enabling micromachining over and/or inside the bulk of materials.[20] The fs (or picosecond) laser can apply ultrashort laser pulses on substrates, minimizing effective heat generation on the inscribed zones. This capability presents precise micromachining approach with the introduction of high localized energy, yielding fast ablation of the materials. During the laser ablation process, the change in topographic surface roughness of polymer substrates can induce surface wettability variations, which depend on the Wenzel or Cassie–Baxter models. The exposed surfaces may undergo a transition from hydrophobic to hydrophilic and vice versa, or they may have their wettability properties controlled depending on the extent of the physical and/or chemical alteration of the ablated areas. Although the surface topography can be significantly affected by laser ablation, the chemistry of the ablated surfaces can also be altered[21] or remain unaffected.[15] Despite having a low throughput operation, laser ablation has the potential to selectively and adaptively tune the surface wettability of microchannels. Other studies have reported the capability of fs laser ablation to modify the surface wettability of PMMA substrates; some inconsistencies exist regarding the effectiveness and accuracy of the conventional technique. Furthermore, the surface wettability of PMMA induced by fs laser ablation, particularly the effects of key parameters, could be characterized. This study investigates surface wettability and topography of fs laser-inscribed PMMA surfaces. It also identifies the anisotropic behaviors associated with surface wettability even after the laser strips are overlapped and proposes an optimized cost-effective fabrication protocol.

2. Results and Discussions

Figure 1a,b displays the experimental and schematic setup used for fs laser micromachining to ablate strips/microchannels. A large was ablated for wettability analysis via overlapping the inscribed lines. The fs laser was first used to fabricate small-scale channels and features (e.g., strips) on surfaces.[22,23] The fs laser efficiently inscribed the surfaces, resulting in strips/microchannels of varying depths and widths when subjected to single beam scans at various fluences. Figure 1c shows that the ablation depth increased as the laser fluence increased. The strip width was also affected by the laser fluence but to a lesser extent than the strip depth (Figure 1d). Consequently, wider microchannels/strips can be generated by applying parallel overlapping laser scans. Achieving a desired strip depth via varying the laser fluence at the single beam scan mode is limited, and larger depths may require multiple scans. Furthermore, to remove material from a surface via ablation, the laser fluence must exceed a certain threshold. For a rough estimate of the laser fluence threshold, the intersection of the fitting curve with the *x*-axis in the plot of strip depth versus laser fluence was obtained (Figure 1e).[15] This *x*-interception value could predict the threshold fluence, which was found to be 9.3 J cm^{-2}. The threshold laser fluence must be between 8.2 J cm^{-2} (ablation) and 13 J cm^{-2} (nonablation), which is consistent with the predicted threshold fluence. Regardless of whether the surface chemistry is altered or not, fs laser ablation induces topographical and morphological changes (e.g., roughness) that may affect surface wettability and alter contact angle (CA) measurements. Therefore, to evaluate the surface wettability of the ablated microchannels/strips resulting from fs laser micromachining, the ablation areas can be enlarged sufficiently to host the liquid droplets for measurements. In this study, the substrates were inscribed vertically along the *y*-axis at specific tuned shifting pitches of the laser beam, resulting in sequential microchannels/strips having various overlaps (Figure 1f). This allowed for the creation of a sufficient ablation area of 4×4 mm^2 for measurements (Figure 1g). It is hypothesized that the laser scanning in a spatially bidirectional mode could potentially affect the wetting behaviors of the laser-inscribed areas. In this regard, the second subsequent raster scanning was carried out in transverse directions with the angles of 0°, 30°, 45°, 60°, and 90° with respect to the original vertical scans. These angles, denoted as "bidirectional scanning angle", θ_{ba}, were applied, and the corresponding process denoted as "bidirectional scanning mode" necessitated two-step scanning operations (Figure 1h). For example, the bidirectional scanning at 90° corresponds to the fs laser raster scans performed vertically along the *y*-axis, followed by the next subsequent scans at an angle of 90° along the *x*-axis.

2.1. Surface Patterns and Roughness

When a substrate surface is subjected to laser ablation, it undergoes topographical and/or morphological changes in the form of

© 2023 The Authors. Advanced Engineering Materials published by Wiley-VCH GmbH

15272648, 2024, 2, Downloaded from https://onlinelibrary.wiley.com/doi/10.1002/adem.202301217 by Koc University, Wiley Online Library on [01/02/2024]. See the Terms and Conditions (https://onlinelibrary.wiley.com/terms-and-conditions) on Wiley Online Library for rules of use; OA articles are governed by the applicable Creative Commons License

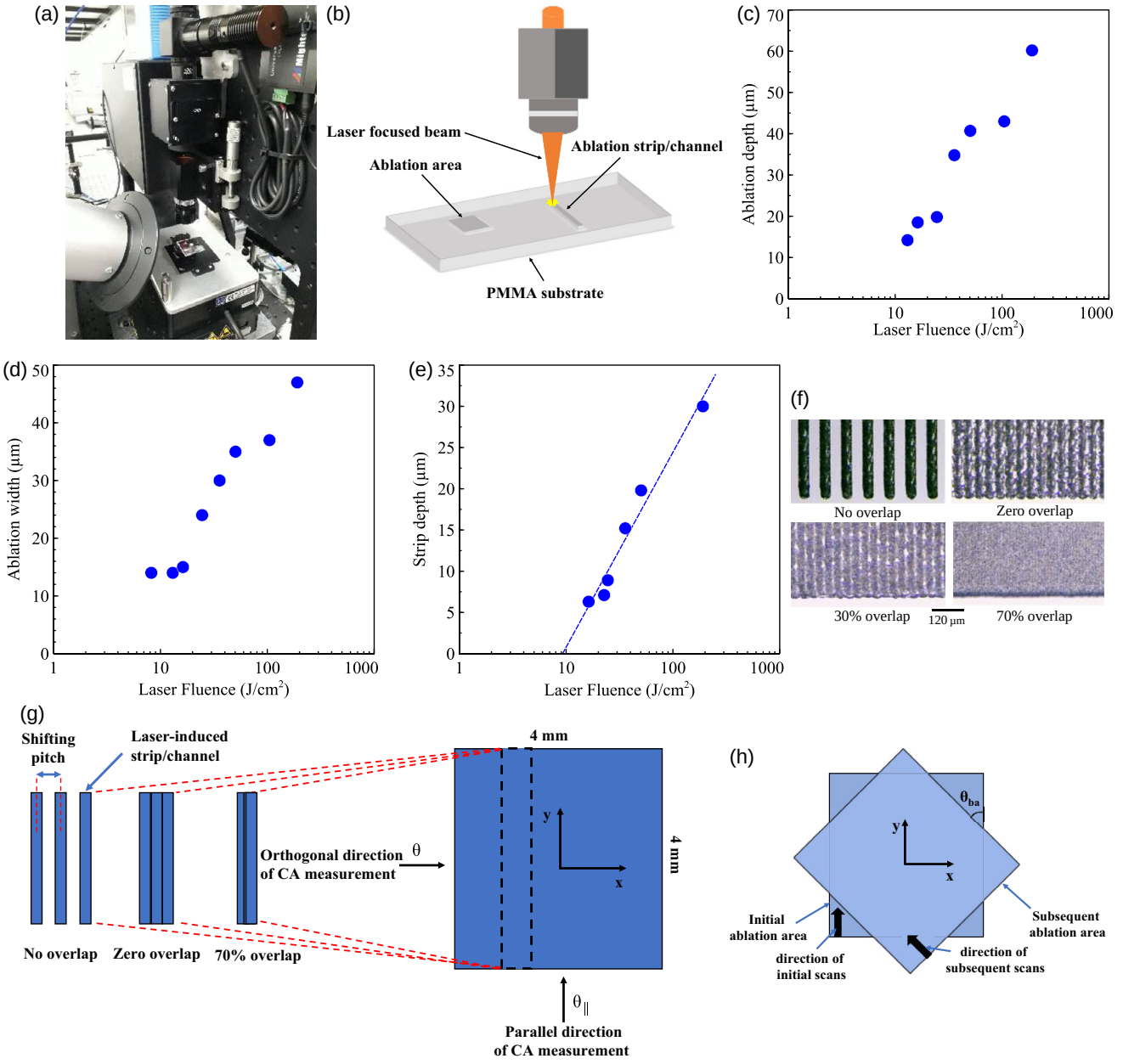


Figure 1. Fs laser ablation system to fabricate microfluidic channels. a) Fs laser system ablating a PMMA substrate. b) Schematic showing fs laser micromachining a strip/channel over a PMMA substrate capable of creating a typical enlarged ablatio area. c) Ablation depth of enlarged laser-produced areas ($4 \times 4\ m^2$) versus laser fluence. d) Ablation width of laser-produced strips/channels versus laser fluence. e) Strip/channel depth versus laser fluence. The experimental data points are fitted with a logarithmic line whose *x*-inception represents a threshold laser fluence of ≈9.3 J cm^{-2}. f) Optical images showing different scan/strip overlaps at laser fluence of 50 J cm^{-2}. g) Schematic descriptions of scan overlaps and directions of CA measurement. h) Schematic of bidirectional scanning mode.

surface roughness and patterns. The surface patterns generated during laser inscription exhibit a directional dependency on the scanning direction (e.g., directional and bidirectional scanning modes). The parameters involved are laser fluence, scanning speed, number of scans, and particularly scan overlap. In directional mode, the typical directional scans are applied only in a specific direction. The utilization of vertical parallel scanning during laser ablation can result in various surface patterns that resemble topographical features such as parallel V-grooves, as observed at low overlaps. Notably, the application of bidirectional mode scanning, implementable by scans applied in two directions, has been investigated. **Figure 2**a illustrates optical microscopy and atomic force microscopy (AFM) maps, depicting the surfaces inscribed at different bidirectional scanning angles, θ_{ba}, with a laser fluence of 50 J cm^{-2} and a scan overlap of 70%. The bidirectional scanning mode manufacturing process

© 2023 The Authors. Advanced Engineering Materials published by Wiley-VCH GmbH

15272648, 2024, 2, Downloaded from https://onlinelibrary.wiley.com/doi/10.1002/adem.202301217 by Koc University, Wiley Online Library on [01/02/2024]. See the Terms and Conditions (https://onlinelibrary.wiley.com/terms-and-conditions) on Wiley Online Library for rules of use; OA articles are governed by the applicable Creative Commons License

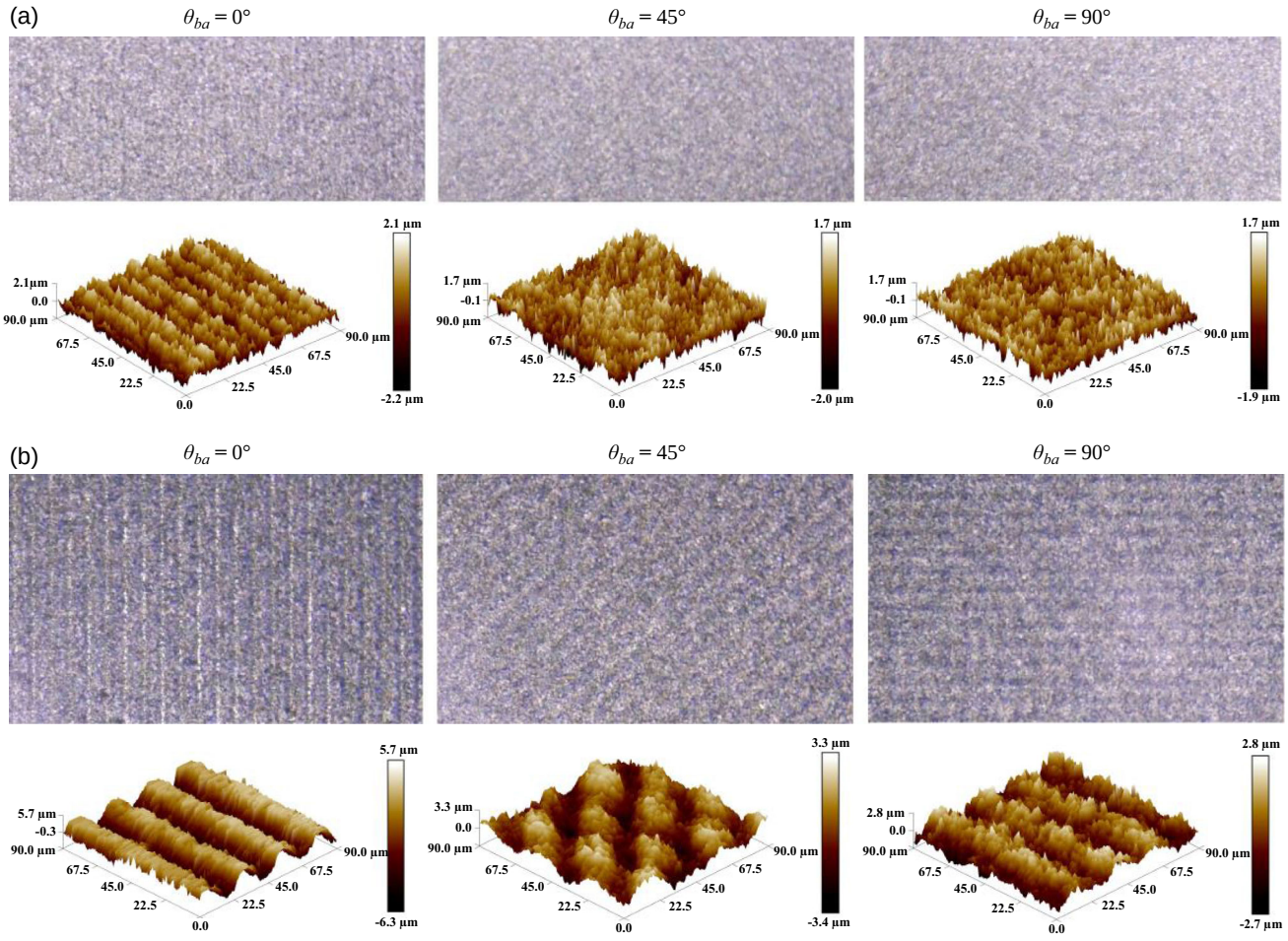


Figure 2. Characterization of the fs laser-ablated surfaces. a) Optical images and AFM maps of fs laser-processed areas produced at laser fluence of 50 J cm^{-2} and scan overlap of 70% at different bidirectional scanning angles. b) Optical images and AFM images of the same conditions but at the scan overlap of 30%. Scale bar: 20 μm.

at angles less than 90° was capable of generating directional patterns. However, inscribing the area at 90° in bidirectional scanning mode could suppress directional patterns and lead to the generation of more isotropic surfaces by enhancing randomized roughness elements. This also results in isotropic wettability, causing droplets sitting on the laser-inscribed areas to form more symmetric shapes. The amount of scan overlap can tremendously interfere with the resulting pattern. At moderate scan overlaps, e.g., 30% overlap, the corresponding optical microscopy and AFM images for the laser fluence of 50 J cm^{-2} illustrate the potential of θ_{ba} in producing new patterns (Figure 2b). Hence, increasing the θ_{ba} from 0° toward 90° can lead to a transition from a V-groove pattern at $\theta_{ba} = 0$ to a tilted V-groove superposed with the woven rattan-like pattern at higher θ_{ba}. Unlike the V-groove structure observed in the case of heterogenous laser ablation (i.e., no scan overlaps in Figure 1f), the newly emerged V-groove structures at various θ_{ba} values are incorporated over the ablated surface.

To demonstrate the effect of the bidirectional scanning angle on the droplet behavior, **Figure 3**a depicts the physical shape of droplets placed on the ablation areas processed at the laser fluence of 50 J cm^{-2} for the scan overlaps of 30% at different θ_{ba}. The photographs show that the droplet in the case of $\theta_{ba} = 0$ is elongated along the *y*-axis (i.e., parallel to the scan direction). When θ_{ba} increases, the elongated droplet follows the direction of the last subsequent scans, which correspond to the bidirectional angle. After increasing θ_{ba} to intermediate values, $0 < \theta_{ba} < 90°$, the degree of droplet elongation decreases before increasing again at $\theta_{ba} = 90°$, where the droplet elongates along the *x*-axis. This behavior is distinct from the other studies,[15] which focused on a wide range of laser fluences without observing any anisotropic wetting behavior. Notably, the observed anisotropic wettability has not been reported in the literature for laser-processed surfaces containing the scan overlap, irrespective of being performed in directional or bidirectional mode. When there is a discontinuity in the laser-inscribed surfaces, i.e., no-overlap case (Figure 1f), anisotropic wetting behaviors are expected.[24] As a result, any droplets placed on such a surface get elongated and stretched over the directional patterned surface. Nevertheless, this behavior is not only limited to nonoverlapping patterns; the pronounced elongated droplets were observed for zero and small scan overlaps as well, as illustrated for the directional scanning mode for the laser fluence of 25 J cm^{-2} (Figure 3b). Overall, the scan overlap in bidirectional

© 2023 The Authors. Advanced Engineering Materials published by Wiley-VCH GmbH

15272648, 2024, 2, Downloaded from https://onlinelibrary.wiley.com/doi/10.1002/adem.202301217 by Koc University, Wiley Online Library on [01/02/2024]. See the Terms and Conditions (https://onlinelibrary.wiley.com/terms-and-conditions) on Wiley Online Library for rules of use; OA articles are governed by the applicable Creative Commons License

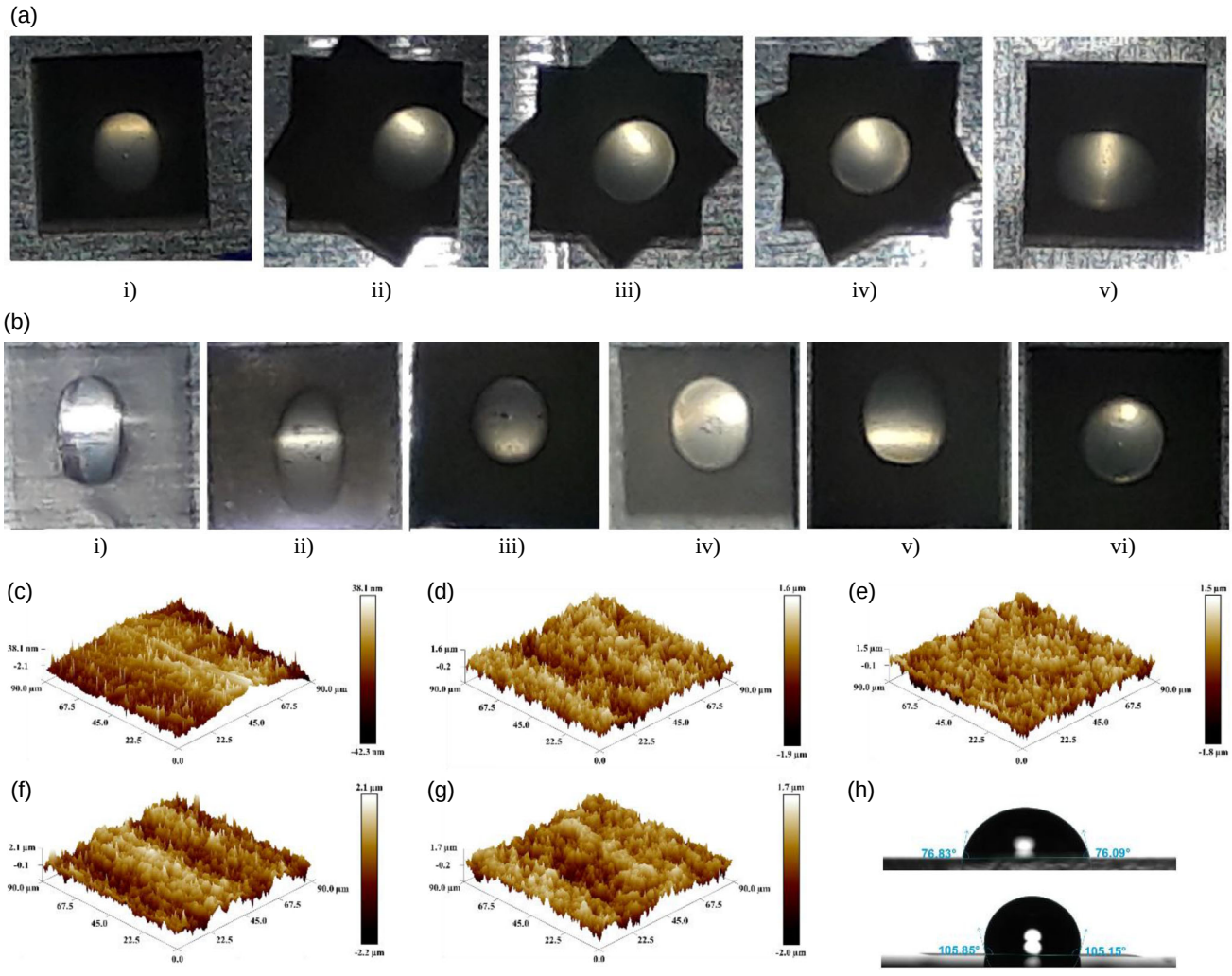


Figure 3. Characterization of wetting properties and CAs. a) Photographs of droplet shapes dropped on PMMA surfaces ablated at laser fluence of 50 J cm^{-2} for bidirectional scanning mode for scan overlap of 30% at different bidirectional scanning angles of i) $\theta_{ab} = 0°$, ii) $\theta_{ab} = 30°$, iii) $\theta_{ab} = 45°$, iv) $\theta_{ab} = 60°$, and v) $\theta_{ab} = 90°$. b) Photographs of droplet shapes at laser fluence of 25 J cm^{-2} for directional mode applied on ablated PMMA surfaces with scan overlaps of i) no-overlap (−100%), ii) zero-overlap (0%), iii) 13%, iv) 30%, v) 50%, and vi) 70%. c–g) AFM maps of untreated PMMA and fs laser-processed PMMA surfaces; c) untreated PMMA (i.e., 0 J cm^{-2}) and different laser fluences at (d) 13, (e) 25, (f) 50, and (g) 191 J cm^{-2} for scan overlap of 70%. h) Photographs of a water CA on an untreated PMMA surface (top) and an ablated PMMA surface (bottom) at laser fluence of 25 J cm^{-2}.

inscription mode showed a remarkable effect on the topographical patterns.

Figure 3c–g represents the AFM maps of the untreated PMMA and fs laser-inscribed PMMA surfaces at different laser fluences with a scan overlap of 70%. The ablated PMMA surfaces undergo significant topographical changes compared to non-treated surfaces. While laser fluence has a notable impact on the depth of the ablated areas (Figure 1c), increasing the fluence does not result in significant variations in roughness. This suggests that the alteration of surface wettability due to laser ablation is predominantly influenced by surface texture and patterns rather than topographic roughness. Additionally, the maximum roughness value (≈1 µm) was associated with surfaces fabricated with the bidirectional scanning mode with a scan overlap of 30% and laser fluence of 50 J cm^{-2}.

2.2. Surface Chemistry

Surface chemistry is a key driving factor to alter surface wettability, as seen in surfaces treated with oxygen plasma.[25] In surfaces inscribed with laser ablation, it has been unclear whether the chemistry of PMMA surfaces is altered after ablation.[15,16] Accordingly, Fourier-transform infrared spectroscopy (FTIR) was used to explore the signs of oxidative degradation through carbonyl index evaluation. FTIR in attenuated total reflection (ATR) mode characterizes the material in close vicinity of the ablation surface by penetrating a sampling depth of 1–2 µm below the examined surface. The carbonyl index is determined by the ratio of absorbance intensities of C═O (1700–1800 cm^{-1}) and C—H (2800–2900 cm^{-1}) stretching regions. The rationale behind the choice of these bands is that the oxidative degradation

© 2023 The Authors. Advanced Engineering Materials published by Wiley-VCH GmbH

15272648, 2024, 2, Downloaded from https://onlinelibrary.wiley.com/doi/10.1002/adem.202301217 by Koc University, Wiley Online Library on [01/02/2024]. See the Terms and Conditions (https://onlinelibrary.wiley.com/terms-and-conditions) on Wiley Online Library for rules of use; OA articles are governed by the applicable Creative Commons License

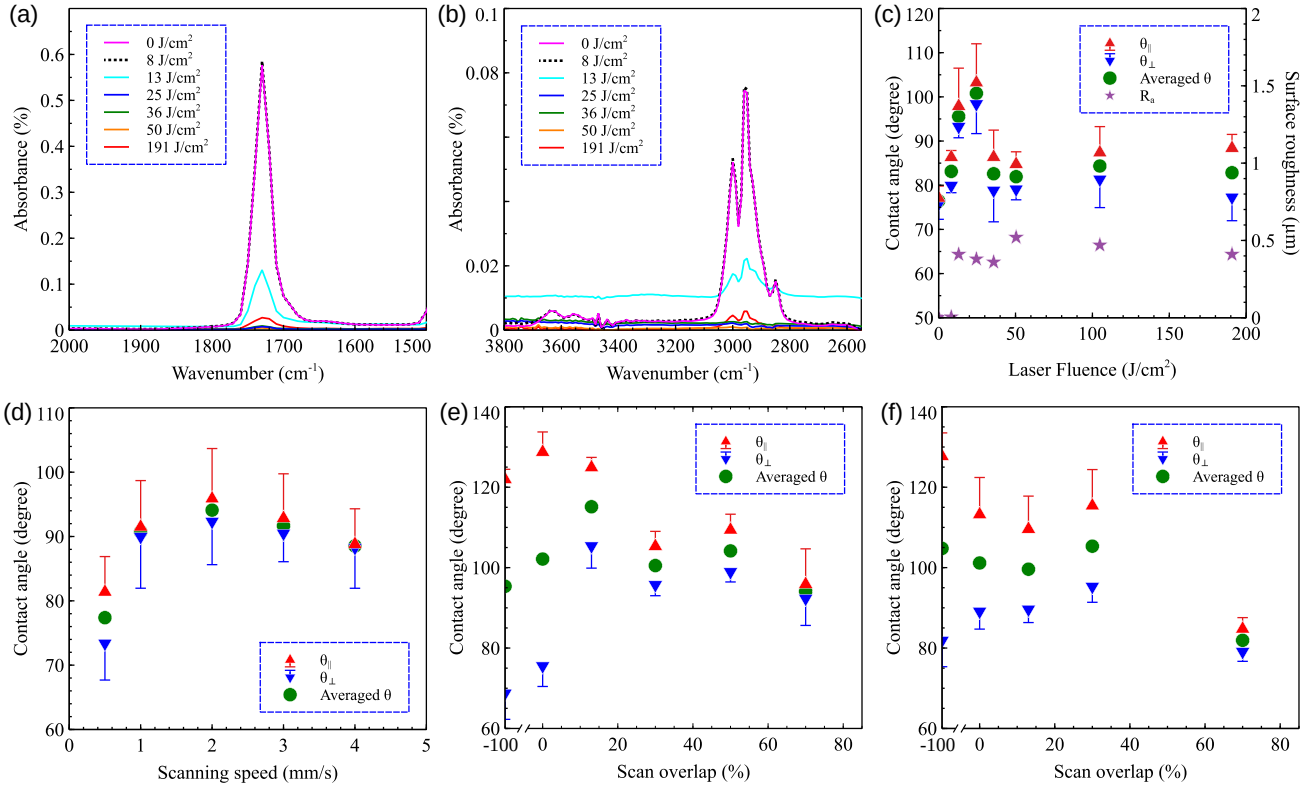


Figure 4. Details corresponding to absorptions of a) C═O stretching and b) C—H stretching for FTIR–ATR spectra of untreated and fs laser-treated PMMA surfaces. c) Static water CA and surface roughness of untreated (at 0 J cm^{-2}) and fs laser-ablated PMMA surfaces versus the laser fluence for the scanning speed of 2 m s^{-1}. d) Static water CA versus laser scanning speed for PMMA surfaces ablated with scan overlap of 70% at laser fluence of 25 J cm^{-2}. CAs versus scan overlap at laser fluences of e) 25 J cm^{-2} and f) 50 J cm^{-2} for the scanning speed of 2 mm s^{-1}.

of polymer necessitates a decrease in C—H intensity and an equivalent increase in the C═O band.[17] **Figure 4**a,b illustrates the ATR infrared spectra of PMMA before and after fs laser ablation, where the peaks at C═O and C—H stretching regions can be obtained to calculate the carbonyl index.

The carbonyl indexes corresponding to the untreated PMMA and the ablated PMMA surfaces at various laser fluences revealed almost no evidence of laser-induced chemical changes on the surfaces after ablation. The carbonyl index remains roughly constant with the increase of the laser fluence (6.2 ± 1.5 J cm^{-2}) for different fluence values (0–191 J cm^{-2}). These results agree with other studies,[15] which found no surface chemistry change upon fs laser ablation. Furthermore, wettability can be attributed to the presence of –OH groups on the surface, which acts as a promoter for water adsorption.[26] Figure 4b demonstrates that the O—H group at the corresponding stretching region (3400–4600 cm^{-1}) does not show any broad absorption peak/band (per laser fluence) ascribing to –OH stretching vibrations. As the surface chemistry does not contribute to the wettability change in the present study, the variations of topographical surface structures control the underlying physics behind surface wetting behaviors.

2.3. Surface Wettability

The anisotropic wetting behavior can be produced due to the heterogeneity existing on a solid surface. This can cause the CA to appear differently when measured along the *y*-axis (denoted by $\theta_{\parallel}$), which is parallel to the initial vertical scanning, versus orthogonal-side measurement along the *x*-axis (denoted by $\theta_{\perp}$) (Figure 1g). For surfaces ablated with the fs laser, the anisotropic wetting behaviors are remarkably prevalent. Several key parameters can affect the surface wettability, exhibiting exceptionally anisotropic wetting behaviors over continuous ablation areas.

2.3.1. Laser Fluence Effect

The wettability of PMMA surfaces irradiated by fs laser can be strongly affected by the laser fluence. The static CA measured on the untreated PMMA is 76° (Figure 3h). However, after the fs laser irradiations, some ablated/residual material debris is deposited on the working surface, which could contribute to the reduced CAs and indicate an artificial hydrophilization.[15] The CA is reduced due to the presence of the material debris on the ablated area (at 53°), compared to the actual value (105°) for the same case after cleaning corresponding to the laser fluence of 25 J cm^{-2} and the scan overlap of 70% (Figure 3h). This indicates that the presence of the PMMA debris disguises the true wettability characteristics of the laser-ablated areas.

In the previously reported studies,[15,16,27] the shifting pitch (i.e., the distance between two subsequent scans) and the number of parallel scans during the manufacturing process have been fixed, while the effect of different laser fluences on the surface

© 2023 The Authors. Advanced Engineering Materials published by Wiley-VCH GmbH

15272648, 2024, 2, Downloaded from https://onlinelibrary.wiley.com/doi/10.1002/adem.202301217 by Koc University, Wiley Online Library on [01/02/2024]. See the Terms and Conditions (https://onlinelibrary.wiley.com/terms-and-conditions) on Wiley Online Library for rules of use; OA articles are governed by the applicable Creative Commons License

wettability was investigated. The main drawback of this conventional method is the mixing up of the scan/strip overlaps when the width dependency of the ablated strips with the laser fluence is considered (Figure 1d). In the present study, the surfaces are ablated by making the constraint of the fixed scan overlaps rather than assuming a fixed shifting pitch and number of parallel scans. Accordingly, the related scanning parameters (i.e., the shifting pitch and the number of parallel scans) were tuned to fulfill the identical scan overlap for each laser fluence. One of the main advantages of this approach is that the number of parallel scans required to ablate the same area could decrease by up to one order of magnitude compared to the conventional methods to reduce manufacturing costs. The effect of laser fluence on the wetting characteristics is shown in Figure 4c, where the static CA is displayed as a function of the laser fluence for the scan overlap of 70% and the scanning speed of 2 mm s^{-1}.

At the laser fluence of 8 J cm^{-2}, there is no ablation on the surface (as validated by the imaging), but rather the corresponding laser-irradiated surface shows iridescent colors when its viewing angle is repeatedly alternated under light illumination. Fs lasers can produce laser-induced periodic surface structures (LIPSSs) on the surface of substrates at fluences below the threshold.[28] Hence, these nanoscale surface structures could act as a diffraction grating that generates iridescent colors.[29,30] Figure S1, Supporting Information, exhibits the iridescence phenomenon observed over the PMMA surface, which is inscribed at a laser fluence of 8 J cm^{-2}. The i–ii panels in Figure S1, Supporting Information, illustrate different moments while slightly varying viewing angles. Although there is no ablation on the surface, the corresponding CA is distinct from the one associated with the untreated PMMA surface, indicating the wettability change due to the laser irradiation in the absence of ablation, which has been reported elsewhere.[31] In contrast to the results reported in the literature, the wettability showed an anisotropic behavior for this case due to the presence of the nanostructure ripple pattern, which is a prevalent form of LIPSSs.

Excluding the data at the laser fluence of 8 J cm^{-2}, where the surface is not ablated, Figure 4c demonstrates that the CA increases with the laser fluence up to 25 J cm^{-2}. Subsequently, the CA suddenly decreases to a certain value by increasing the laser fluence to 36 J cm^{-2}, beyond which saturation is reached, i.e., the CA remains almost constant for laser fluences higher than that value. In Figure 4c, the roughness increases when the ablation occurs as seen by the difference between corresponding roughness values for the smooth PMMA surface and the ablated PMMA surfaces. However, the surface roughness does not considerably change with the increase in the laser fluence within the studied ablation range. This indicates that the topographical patterns/texture induced by fs laser is a driving factor for the surface wettability change, rather than the amount of roughness.

For wettability analysis of rough surfaces, two models have been developed to describe the liquid state in contact with a solid surface. These models are the Wenzel and Cassie–Baxter.[32] In the Wenzel model (Figure S2a, Supporting Information), liquids (e.g., droplets) tend to get through asperities and irregularities underneath the contacted surface, where complete wetting occurs. Wenzel's model suggests that the surface wetting property, either hydrophobic or hydrophilic, is enhanced with increasing roughness. Hence, the CA decreases for an initially hydrophilic surface and increases for an initially hydrophobic surface when the degree of roughness becomes greater. In the Cassie–Baxter model (Figure S2b, Supporting Information), by contrast, liquids do not completely wet the surface, and therefore, air pockets trap between the resting liquids and the actual rough surface. Accordingly, the liquid interface becomes composite, sharing interface with both solid and air. The Cassie–Baxter model predicts that increasing surface roughness always favors increased CA, no matter what the initial wettability behavior is (hydrophilic or hydrophobic).

In the context of these models and considering the moderately hydrophilic nature of PMMA surfaces, the increasing trend of CA with the laser fluence at low laser fluences indicates compliance of the droplet behavior with the Cassie–Baxter model although a slight anisotropic wettability is observed. The presence of strong anisotropic wettability requires a liquid volume to completely wet asperities of the surface and fill the empty spaces, which is consistent with the Wenzel model. For low laser fluences above the threshold, as the anisotropic wettability is not comparatively large, the Cassie–Baxter model can be assumed to generally describe the wetting behavior. Therefore, some air pockets are expected to be trapped between the surface of roughness structures and the interface of the droplets. At the laser fluence of 36 J cm^{-2} and larger, the CA remains constant, which cannot be solely explained by the Cassie–Baxter model. At these laser fluences, the anisotropic wetting behavior becomes more enhanced, indicating partial wetting of the rough surfaces. In this case, wetting behavior is thought to be partial, not complete, because with complete wetting, as described by the Wenzel model, the CAs should have been decreased with the laser fluence for an initially hydrophilic PMMA surface. Hence, a mixed state (consisting of Wenzel and Cassie–Baxter models) could be ascribed to the wetting behavior, shifting from the Cassie–Baxter state to the mixed state wetting regime when the laser fluence is increased.

2.3.2. Laser Scanning Speed Effect

To understand the laser scanning speed effect on the surface wettability, the conventional method was initially utilized to ablate the surface. Hence, the number of parallel scans along the vertical direction (i.e., *y*-axis) and the shifting pitch were constant at 533 and 7.5 μm, respectively. This resulted in different scan overlaps (ranging from 83% to 61%) as the scanning speed was varied from 0.2 to 4.0 mm s^{-1}. A change in the scanning speed can be equivalent to an appropriate change in the laser fluence. This relationship can be observed in Figure S3a,b, Supporting Information, where the width of the strips and the depth of the ablation areas are separately displayed for both the scanning speed (laser fluence: 25 J cm^{-2}) and the laser fluence (scanning speed: 2 mm s^{-1}). For instance, the scanning speed of 1 mm s^{-1} can be roughly correlated with the laser fluence of 36 J cm^{-2} if both the width of the strips and the depth of the ablation areas are considered. The depth of the strips or microchannels as a function of the scanning speed (Figure S4, Supporting Information) shows a similar trend to the depth of the ablation areas versus the scanning speed. The material removal from the surface is

© 2023 The Authors. Advanced Engineering Materials published by Wiley-VCH GmbH

15272648, 2024, 2, Downloaded from https://onlinelibrary.wiley.com/doi/10.1002/adem.202301217 by Koc University, Wiley Online Library on [01/02/2024]. See the Terms and Conditions (https://onlinelibrary.wiley.com/terms-and-conditions) on Wiley Online Library for rules of use; OA articles are governed by the applicable Creative Commons License

reduced at higher scanning speeds, where marginal depth variation is observed.

The variation of the CA versus the laser scanning speed, driven by moving the translational platform on which the samples are held, is depicted in Figure 4d for a laser fluence of 25 J cm^{-2}. Increasing the laser scanning speed results in the dramatic increase of the CA up to the speed of 1 mm s^{-1} beyond which the opposite behavior is observed, but to a lesser extent. The optical microscopy images (Figure S5a, Supporting Information) qualitatively illustrate that despite the large scan/strip overlaps falling within the range between 61% and 80%, the material removal from the PMMA surface occurring at high scanning speed, i.e., 4 mm s^{-1}, is not as effective as the ablation at 0.5 mm s^{-1}. The ablation depth of the laser-inscribed areas shown in Figure S3b, Supporting Information, supports this photographic deduction. A possible explanation could be traced in the analysis of the pulse overlap over a spot size, and thereby the number of incident laser pulses received per spot site. The laser scanning speed variation engenders the contribution of the number of pulses spatially overlapped within one spot size. The laser overlap ratio per one spot can be calculated by (Figure S6, Supporting Information)

$$\left(1 - \frac{v_s}{R \times d}\right) \times 100\% \quad (1)$$

where v_s is the laser scanning speed, d is the spot size diameter, and R is the repetition rate (1 kHz). When the laser scanning speed is high, the laser pulse could achieve no overlap condition at the spot site, receiving only a single incident laser pulse. By contrast, the pulse overlap per spot size could approach 100% at low scanning speeds, allowing the maximum number of pulses to hit the same spot. Hence, the laser can ablate more materials from the substrate at the spot site, yielding deeper microchannels/strips per laser scan. The decrease in the scanning speed led to the increased strip width (Figure S3a, Supporting Information), thereby resulting in increased strip overlaps, which consequently affected the resulting patterns on the surfaces. This observation is supported by the optical images and their corresponding AFM maps (Figure S5a,b, Supporting Information). Besides, a slight change in the surface roughness was discernable with the average surface roughness, R_a, of 445 nm measured at the scanning speed of 0.5 mm s^{-1} compared to 308 nm at 4 mm s^{-1}. Compared to other scan speeds, at the scan speed of 0.5 mm s^{-1}, the anisotropic wetting behavior was observed, despite the corresponding large scan overlap (about 80%) associated. This finding is consistent with the increased anisotropic behavior at high laser fluences (Figure 4c). The high laser fluence can be regarded as analogous to a small scanning speed in terms of the ablation process (Figure S3, Supporting Information). The results of applying fixed scan overlap through tuning the shifting pitch are expected to be qualitatively similar to those of varying the laser fluences at constant scan overlaps.

2.3.3. Scan Overlap Effect

The laser striping method with strips decorated separately on a surface has proved to be a significant parameter revealing anisotropic wetting behavior.[24] However, this behavior has not been reported for the strips making overlaps yet. In this work, we have systematically studied the influence of the strip overlap on surface-wetting behaviors. When a surface is processed with the laser striping at which the strips are separated by certain distances (i.e., no strips overlap case), a heterogeneity in the surface is produced, which is identified as a directional patterned surface.[1] This potentially leads to the appearance of the anisotropic behaviors in the surface wettability, an effect that resembles what the chemical heterogeneity can generate.[33] Our results revealed that the anisotropic wettability is not exclusively limited to the case of separated strips, i.e., no overlap case, but can also be observed at relatively large strip/scan overlaps. Figure 4e–f demonstrates the surface wettability of the ablation areas characterized by the CA as a function of the scan/strip overlap for the laser fluences of 25 and 50 J cm^{-2} at the scanning speed of 2 mm s^{-1}. The experimental data showing the anisotropic wettability in the case of "no-scan overlap" are in agreement with the literature results.[24] It is worth noting that a negative value for scan overlap percentage indicates the degree to which laser-processed strips are separated from each other. These figures also clearly highlight the influence of the strip/scan overlap on the anisotropic CAs. A scan overlap that is too large results in isotropic surface wettability, whereas a scan overlap that is varied from small to relatively large overlaps leads to anisotropic wettability, and accordingly anisotropic CAs. As the scan overlap increases, the surfaces tend to show less anisotropic behaviors, turning to complete isotropic wetting at the largest strip overlap. The V-groove structures effect gradually diminishes with increasing the strip overlap (Figure 1f), transforming toward a more isotropic randomized arrangement of roughness elements at large strip overlap. While the scan/strip overlap exhibits a significant influence on the degree of wetting anisotropy, apart from the reduced CA observed at the largest scan overlaps, a definitive conclusion regarding its direct impact on wettability (i.e., hydrophilicity and hydrophobicity) cannot be drawn.

2.3.4. Effects of Bidirectional Scanning Angle and Scan Repetition

As a different manufacturing strategy, the fs laser has the capability of scanning in multiple directions. Performing the ablation in bidirectional mode at the bidirectional scanning angle of 90°, $\theta_{bs} = 90°$, (i.e., the laser ablation occurs sequentially along both the y-axis and x-axis in order) has been previously carried out[15] to reduce the surface roughness dependency to the scanning direction, thereby rendering roughness toward randomized and isotropic features. Accordingly, we hypothesized that scanning in a bidirectional mode with different bidirectional scanning angles may present new schemes in wetting behavior and characteristics. In this regard, we performed the bidirectional scanning at various θ_{bs} (from 0° to 90°) to generate the ablation areas for wettability analysis. In **Figure 5**a,b, the CA as a function of θ_{bs} is displayed for the laser fluences of 25 and 50 J cm^{-2}, respectively, while keeping the scanning speed and the scan overlap fixed at 2 mm s^{-1} and 70%, respectively. Among the different bidirectional scanning angles evaluated, $\theta_{bs} = 0°$ corresponds not only to the angle of 0° between the

© 2023 The Authors. Advanced Engineering Materials published by Wiley-VCH GmbH

15272648, 2024, 2, Downloaded from https://onlinelibrary.wiley.com/doi/10.1002/adem.202301217 by Koc University, Wiley Online Library on [01/02/2024]. See the Terms and Conditions (https://onlinelibrary.wiley.com/terms-and-conditions) on Wiley Online Library for rules of use; OA articles are governed by the applicable Creative Commons License

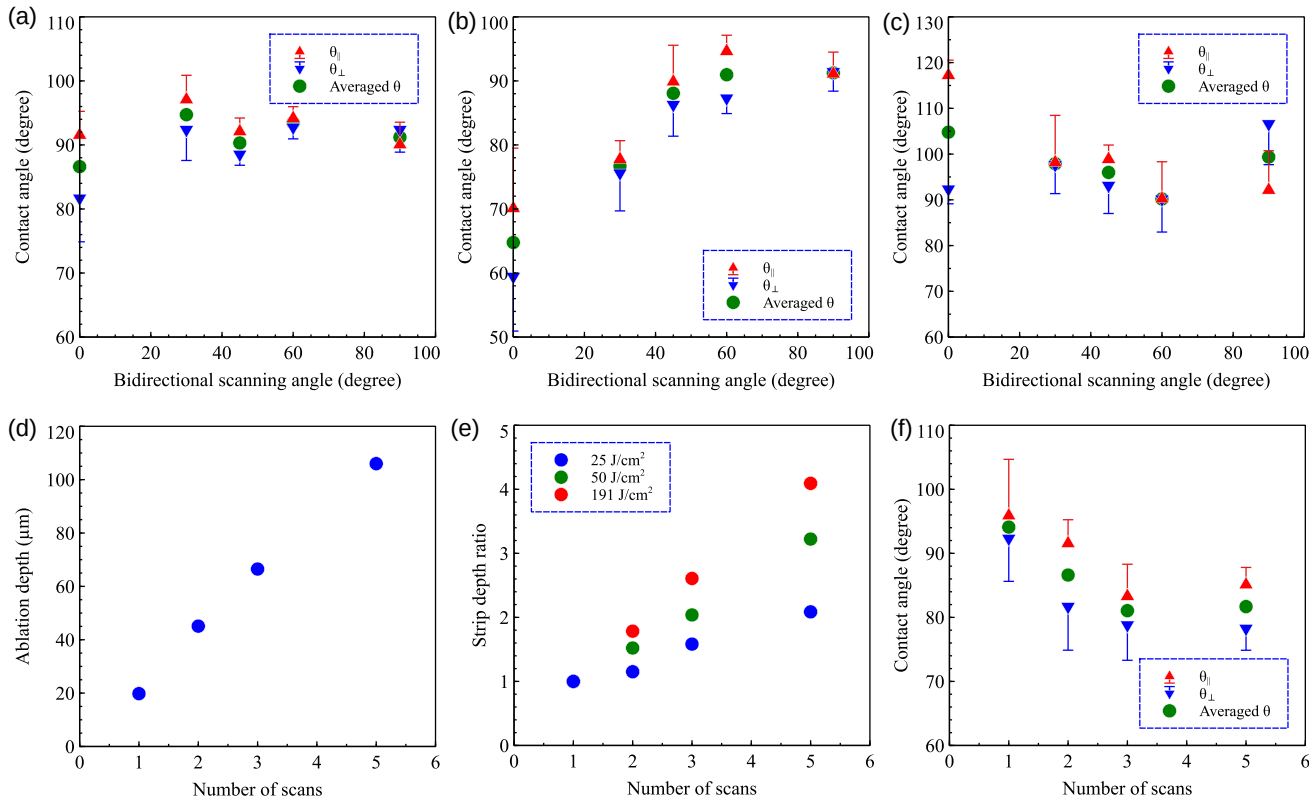


Figure 5. CA versus bidirectional scanning angles for a) scan overlap of 70% and laser fluence of 25 J cm^{-2}, b) scan overlap of 70% and laser fluence of 50 J cm^{-2}, and c) scan overlap of 30% and laser fluence of 50 J cm^{-2}. d) Ablation depth of enlarged laser produced areas (4 × 4 m^2) versus number of scans at laser fluence of 25 J cm^{-2} and scan overlap of 70%. e) Strip depth ratio of ablation after a certain number of scans relative to a single scan as a function of the number of scans for different laser fluences at the scanning speed of 2 mm s^{-1}. f) CA versus number of scans at laser fluence of 25 J cm^{-2} and scan overlap of 70% at the scanning speed of 2 mm s^{-1}.

two subsequent scans but also indicates the case where the laser ablation is applied to the surface twice under the same condition. Figure 5b illustrates that the laser ablation in the bidirectional mode has a positive effect on the modification of the surface wettability for the laser fluence of 50 J cm^{-2}. In this particular case, the transition in the surface wettability, shifting from the onset of hydrophobicity to moderate hydrophilicity, occurs via varying θ_{bs} from 90° to 0°, resulting in the most hydrophilic surface. Conversely, the surface wettability remains roughly unaffected with the variation in bidirectional scanning angle for the laser fluence of 25 J cm^{-2} (Figure 5a), where the CA deviation remains within a narrow range of 10%. Furthermore, the anisotropic wetting behavior is more pronounced at lower values of θ_{bs}. The scan overlap showed a distinctive behavior as well. The experimental data for the scan overlap of 30% at a laser fluence of 50 J cm^{-2} (Figure 5c) indicated that the surfaces exhibited strong anisotropic wetting behaviors at both ends of the bidirectional scanning angle range (i.e., $\theta_{bs} = 0°$ and $\theta_{bs} = 90°$), whereas the dominant state in the intermediate θ_{bs} (i.e., $0° < \theta_{bs} < 90°$) was characterized by the isotropic wettability. Furthermore, the preferential spreading of droplets was observed along the direction of the latter laser processing. When comparing the CAs measured across the laser-processed areas for $\theta_{bs} = 0°$ and $\theta_{bs} = 90°$, the anisotropic wettability direction and the corresponding elongation of droplets align with the latest scanning direction of the two subsequent scanning processes for each respective θ_{bs}, which were along y-axis and x-axis, respectively.

Similar to the laser fluence and the scanning speed, the repetition of the scans for ablating an area can significantly influence its depth (e.g., a strip or an enlarged ablated area). Exerting multiple scans can result in an increased ablation depth. Figure 5d presents the depth of the laser ablation area versus the number of scans for the scan overlap of 70% at the laser fluence of 25 J cm^{-2}. This figure highlights that the ablation depth increases as the number of scans is increased. Thus, the scan repetition, serving as a significant parameter, allows for the controlled tuning of the depth of an ablation area, as long as a saturation state has not been reached. The saturation means that the depth of ablation areas is no longer increased with the scan repetition. Likewise, the same principle applies to the depth of strips varying with the number of scans. It is expected that the incremental trend will eventually reach a plateau, representing a saturation state, by repeating the ablation process multiple times.[34,35] Furthermore, each laser fluence leads to a distinct plateau. Figure 5e presents the strip depth ratio of ablation after a certain number of scans relative to a single scan as a function of the "number of scans" for different laser fluences at the scanning speed of 2 mm s^{-1}. The higher the laser fluence amplifies the

© 2023 The Authors. Advanced Engineering Materials published by Wiley-VCH GmbH

15272648, 2024, 2, Downloaded from https://onlinelibrary.wiley.com/doi/10.1002/adem.202301217 by Koc University, Wiley Online Library on [01/02/2024]. See the Terms and Conditions (https://onlinelibrary.wiley.com/terms-and-conditions) on Wiley Online Library for rules of use; OA articles are governed by the applicable Creative Commons License

impact of scan repetitions on the strip depth, i.e., the higher the laser fluence the larger the strip depth ratio. Apart from its effect on the ablation depth, the scan repetition has also demonstrated the ability to modify the surface wettability for the scan overlap of 70% and the laser fluence of 25 J cm^{-2} (Figure 5f). Employing the laser ablation on a surface multiple times could enhance its hydrophilicity up to a certain scan repetition beyond which no change in the wetting behavior is observed. The corresponding topographical images (AFM maps in Figure S7, Supporting Information) provide further evidence that the scan repetition would potentially enhance the scan directionality effect through which the anisotropic behavior is augmented while overall reducing the surface wettability.

3. Conclusion

Fs laser ablation has been utilized to modulate the surface properties of PMMA as a ubiquitous material in microfluidic devices. A comprehensive parameter study demonstrated that the fs laser ablation can modify the wettability behavior of PMMA. This can lead to a conversion from moderate hydrophilicity to hydrophobicity, or to a partial enhancement of hydrophilicity. The laser ablation can inherently generate anisotropic wettability even for laser ablation areas processed in a continuous fashion. This methodology for manufacturing the large ablation areas based on tuned associated parameters offers a cost-effective approach compared to the conventional methods. This approach, taking all involved parameters into account, is a modified version of the formation of surface structures. Furthermore, the topographical and chemical analysis of the ablation surfaces confirmed that the laser-induced texture and patterns were responsible for the wettability change of the surfaces rather than the surface chemistry and roughness. The laser ablation technique not only can generate structures, such as microchannels, that are well suited for swift integration in microfluidics applications but can also be utilized to modify surface wettability. By adjusting both manufacturing and laser parameters, anisotropic and isotropic wettability properties can be achieved on ablated surfaces.

4. Experimental Section

Equipment: To ablate PMMA substrates, a fs laser system (Spectra-Physics Spitfire Ace) was employed generating 120 fs pulses at an 800 nm center wavelength, 1 kHz repetition rate. The focal length of the lens was 50 mm through which the laser beam focused on the surface of samples, giving the laser beam spot radius of $w_0 = 6$ μm. The laser pulse was linearly polarized and had a maximum pulse energy of 4 mJ. A software-controlled translation stage was used to guide and translate samples to predetermined paths and locations. The translational speed of the working platform was adjusted between 0 and 4 mm s^{-1}, while the acceleration speed was set at 5 mm s^{-1}.

An optical CA meter (Biolin Scientific Attension Theta Lite TL101-Auto1) was used, which records drop images and analyzes the drop shape automatically. It measures the static CA based on the sessile drop method with the aid of interface software that serves the Young–Laplace fitting to determine the CA in its drop shape analysis. As the ablation technique causes the exposed substrates to be roughened and textured, the roughness features and patterns were qualitatively characterized by an optical microscope.

An AFM (Bruker Dimension Icon) device was employed to map the quantitative measurements of the topographical surface roughness in noncontact mode. To understand whether the ablated surfaces undergo any surface chemistry changes, the FTIR was applied before and after fs laser irradiation. The measurements were obtained with the FTIR in the ATR mode (Thermo Scientific iS10 FT-IR) while the air was taken as the background. The spectra were collected (with the 256 sequential scans and the resolution of 2 cm^{-1} for noise reduction) in the wavenumber ranging from 700 to 4000 cm^{-1}. The ablation depth of each 4×4 m^2 ablated area were measured by a profilometer (Dektak XT-S Stylus Profiler), while the depth of strips/microchannels was estimated via using a white light interferometer (Bruker ContourGT white light interferometer).

Materials, Sample Preparation, and Experimental Procedure: PMMA sheets with a thickness of 2 mm were used and the Milli-Q water was used as the working liquid for CA measurements.

Before performing any experiments, the ablated PMMA samples were cleaned by sonicating for 15 min inside a Milli-Q water bath, followed by drying on a heater plate for 30 min at 50 °C. The surface wettability was assessed by measurement of the static CAs of water droplets (2.5 μL) sitting on the ablation areas. Each measurement was repeated at least 5 times to ensure the reliability and repeatability of the CA measurements. To check the repeatability of the fs laser method, some samples with the same protocol were prepared (two for each case), and their CAs were measured as well. The error bars in the figures represent either the variation in CA measurements or their combination with sample repetitions, if applicable. In the case of sample repetition, it was obtained that the CA values exhibited a variation ranging from 3% to 20%.

Supporting Information

Supporting Information is available from the Wiley Online Library or from the author.

Acknowledgements

M.S. acknowledges the support from Co-Funded Brain Circulation2 Scheme (CoCirculation2) program. M.S. also acknowledges TÜBİTAK-BİDEB, the Science Fellowships and Grant Programmes Department within TÜBİTAK. S.T. acknowledges TÜBİTAK 2232 International Fellowship for Outstanding Researchers Award (118C391), Alexander von Humboldt Research Fellowship for Experienced Researchers, Marie Skłodowska-Curie Individual Fellowship (101003361), and Royal Academy Newton-Katip Çelebi Transforming Systems Through Partnership award for financial support of this research. Opinions, interpretations, conclusions, and recommendations are those of the authors and are not necessarily endorsed by the TÜBİTAK. This work was partially supported by Science Academy's Young Scientist Awards Program (BAGEP), Outstanding Young Scientists Awards (GEBİP), and Bilim Kahramanlari Dernegi The Young Scientist Award. This study was conducted using the service and infrastructure of Koç University Translational Medicine Research Center (KUTTAM) and Koç University Surface Science and Technology Center (KUYTAM). M.S. also is so much thankful to the kind support of KUTTAM and KUYTAM staff, in particular the KUYTAM staff members during the project. The authors have no other relevant affiliations or financial involvement with any organization or entity with a financial interest in or financial conflict with the subject matter or materials discussed in the article apart from those disclosed.

Conflict of Interest

The authors declare no conflict of interest.

 © 2023 The Authors. Advanced Engineering Materials published by Wiley-VCH GmbH

15272648, 2024, 2, Downloaded from https://onlinelibrary.wiley.com/doi/10.1002/adem.202301217 by Koc University, Wiley Online Library on [01/02/2024]. See the Terms and Conditions (https://onlinelibrary.wiley.com/terms-and-conditions) on Wiley Online Library for rules of use; OA articles are governed by the applicable Creative Commons License

Data Availability Statement

The data that support the findings of this study are available from the corresponding author upon reasonable request.

Keywords

anisotropic wettability, femtosecond lasers, laser ablation, surface functionalization

Received: August 7, 2023
Revised: November 21, 2023
Published online: December 7, 2023

[1] D. Xia, L. M. Johnson, G. P. Lōpez, *Adv. Mater.* **2012**, *24*, 1287.
[2] P. Ge, S. Wang, J. Zhang, B. Yang, *Mater. Horiz.* **2020**, *7*, 2566.
[3] H. Bai, L. Wang, J. Ju, R. Sun, Y. Zheng, L. Jiang, *Adv. Mater.* **2014**, *26*, 5025.
[4] C. Dorrer, J. Rühe, *Langmuir* **2008**, *24*, 6154.
[5] Y. Lai, F. Pan, C. Xu, H. Fuchs, L. Chi, *Adv. Mater.* **2013**, *25*, 1682.
[6] Z. Yu, F. F. Yun, Y. Wang, L. Yao, S. Dou, K. Liu, L. Jiang, X. Wang, *Small* **2017**, *13*, 1701403.
[7] J. Lai, B. Sunderland, J. Xue, S. Yan, W. Zhao, M. Folkard, B. D. Michael, Y. Wang, *Appl. Surf. Sci.* **2006**, *252*, 3375.
[8] F. Darain, M. A. Wahab, S. C. Tjin, *Anal. Lett.* **2012**, *45*, 2569.
[9] K. Nagato, N. Takahashi, T. Shimura, M. Nakao, *CIRP Ann.* **2019**, *68*, 587.
[10] F. Zhang, H. Y. Low, *Langmuir* **2007**, *23*, 7793.
[11] D. Zhang, F. Chen, G. Fang, Q. Yang, D. Xie, G. Qiao, W. Li, J. Si, X. Hou, *J. Micromech. Microeng.* **2010**, *20*, 075029.
[12] J. Yong, F. Chen, Q. Yang, X. Hou, *Soft Matter* **2015**, *11*, 8897.
[13] K. H. Chu, R. Xiao, E. N. Wang, *Nat. Mater.* **2010**, *9*, 413.
[14] N. A. Malvadkar, M. J. Hancock, K. Sekeroglu, W. J. Dressick, M. C. Demirel, *Nat. Mater.* **2010**, *9*, 1023.
[15] C. De Marco, S. M. Eaton, R. Suriano, S. Turri, M. Levi, R. Ramponi, G. Cerullo, R. Osellame, *ACS Appl. Mater. Interfaces* **2010**, *2*, 2377.
[16] Z. K. Wang, H. Y. Zheng, C. P. Lim, Y. C. Lam, *Appl. Phys. Lett.* **2009**, *95*, 111110.
[17] R. Suriano, A. Kuznetsov, S. M. Eaton, R. Kiyan, G. Cerullo, R. Osellame, B. N. Chichkov, M. Levi, S. Turri, *Appl. Surf. Sci.* **2011**, *257*, 6243.
[18] K. Sugioka, J. Xu, D. Wu, Y. Hanada, Z. Wang, Y. Cheng, K. Midorikawa, *Lab Chip* **2014**, *14*, 3447.
[19] G. Pozza, S. Kroesen, G. Bettella, A. Zaltron, M. Esseling, G. Mistura, P. Sartori, E. Chiarello, M. Pierno, C. Denz, C. Sada, *Optofluid. Microfluid. Nanofluid.* **2014**, *1*, 34.
[20] T. N. Kim, K. Campbell, A. Groisman, D. Kleinfeld, C. B. Schaffer, *Appl. Phys. Lett.* **2005**, *86*, 201106.
[21] K. Yin, L. Wang, Q. Deng, Q. Huang, J. Jiang, G. Li, J. He, *Nano-Micro Lett.* **2022**, *14*, 97.
[22] D. H. Kam, L. Shah, J. Mazumder, *J. Micromech. Microeng.* **2011**, *21*, 045027.
[23] R. Moreddu, V. Nasrollahi, P. Kassanos, S. Dimov, D. Vigolo, A. K. Yetisen, *Small* **2021**, *17*, 2102008.
[24] F. Chen, D. Zhang, Q. Yang, X. Wang, B. Dai, X. Li, X. Hao, Y. Ding, J. Si, X. Hou, *Langmuir* **2011**, *27*, 359.
[25] R. Morent, N. De Geyter, C. Leys, L. Gengembre, E. Payen, *Surf. Interface Anal.* **2008**, *40*, 597.
[26] S. Yamamoto, K. Andersson, H. Bluhm, G. Ketteler, D. E. Starr, T. Schiros, H. Ogasawara, L. G. M. Pettersson, M. Salmeron, A. Nilsson, *J. Phys. Chem. C* **2007**, *111*, 7848.
[27] Z. K. Wang, H. Y. Zheng, H. M. Xia, *Microfluid. Nanofluid.* **2011**, *10*, 225.
[28] M. Birnbaum, *J. Appl. Phys.* **1965**, *36*, 3688.
[29] A. Y. Vorobyev, C. Guo, *Appl. Phys. Lett.* **2008**, *92*, 041914.
[30] B. Sarrat, C. Pécheyran, S. Bourrigaud, L. Billon, *Langmuir* **2011**, *27*, 3174.
[31] H. Qi, T. Chen, L. Yao, T. Zuo, *Microfluid. Nanofluid.* **2008**, *5*, 139.
[32] P. Roach, N. J. Shirtcliffe, M. I. Newton, *Soft Matter* **2008**, *4*, 224.
[33] H. P. Jansen, K. Sotthewes, C. Ganser, C. Teichert, H. J. W. Zandvliet, E. S. Kooij, *Langmuir* **2012**, *28*, 13137.
[34] M. Henn, M. Buser, V. Onuseit, R. Weber, T. Graf, in *Procedia CIRP*, Elsevier B.V., Fürth, Germany **2022**, p. 61.
[35] D. Lee, *J. Weld. Joining* **2018**, *36*, 50.

© 2023 The Authors. Advanced Engineering Materials published by Wiley-VCH GmbH

15272648, 2024, 2, Downloaded from https://onlinelibrary.wiley.com/doi/10.1002/adem.202301217 by Koc University, Wiley Online Library on [01/02/2024]. See the Terms and Conditions (https://onlinelibrary.wiley.com/terms-and-conditions) on Wiley Online Library for rules of use; OA articles are governed by the applicable Creative Commons License